THE JOURNAL OF BIOLOGICAL CHEMISTRY
Vol. 271, No. 19, Issue of May 10, pp. 11291–11300, 1996
Printed in U.S.A.

Kinetics of Fatty Acid Interactions with Fatty Acid Binding Proteins from Adipocyte, Heart, and Intestine*

(Received for publication, January 31, 1996)

Gary V. Richieri, Ronald T. Ogata, and Alan M. Kleinfeld‡

From the Medical Biology Institute, La Jolla, California 92037

Rate constants for the interaction of fatty acids (FA) with fatty acid binding proteins (FABP) from adipocyte (A-FABP), heart (H-FABP), and intestine (I-FABP) were determined by using stopped-flow fluorometry and ADIFAB, the fluorescent probe of free fatty acids (FFA), or a new FFA probe, ADIFAB2, constructed by derivatizing with acrylodan the Leu^{72} → Ala mutant of I-FABP. ADIFAB2, because its binding affinities are about 10-fold greater than ADIFAB, was found to be more accurate for monitoring the kinetics of the higher affinity reactions. On- (k_{on}) and off- (k_{off}) rate constants were determined as a function of temperature. Our results reveal that in all cases the FA-FABP equilibrium is achieved within 2 s at 37 °C and within 20 s at 10 °C. Off-rate constants varied by about 10-fold among the different underivatized FABPs; k_{off} values were smallest for H-FABP and largest for A-FABP, while k_{on} values for these proteins generally varied by less than 2-fold. The results show that the previously reported larger affinities of I- and H-FABPs as compared to A-FABP are primarily a reflection of larger k_{on} values for I-FABP and smaller k_{off} values for H-FABP. Eyring transition state theory was used to evaluate the activation thermodynamic parameters for both on- and off-reactions and the results show that in virtually all cases the rate-limiting steps are predominately enthalpic. Activation free energies for binding to ADIFAB are generally composed of about 8 kcal/mol unfavorable enthalpy and about a 1 kcal/mol favorable entropic contribution. For the underivatized FABPs the activation free energies are all about 7 ± 0.3 kcal/mol, suggesting that the transition state for entering or leaving the binding site involves a common protein structural change. We suggest that entering or leaving the FABP binding cavity involves similar mechanisms for all 3 FABPs and may involve amino acid residues located within the portal regions of these proteins.

Fatty acid binding proteins (FABP)[1] are a family of 14–15-kDa proteins found in the cytosols of various cells (1–8). Although the three-dimensional structures of these proteins are similar, individual members of this family exhibit considerable variation in their amino acid sequences (9–12). In addition, the conformation of the fatty acid (FA) within the binding site differs for different FABPs and, to varying degrees, for different FA within the same protein (9–12). Consistent with these amino acid sequence and FA conformational differences, we have recently found considerable differences in the binding affinities of FA to FABPs from adipocyte, heart, and intestine (12–14). Using the fluorescent probe ADIFAB, we found that equilibrium binding constants differ by about 3 orders of magnitude, depending upon FA and FABP type. This heterogeneity was also reflected in the equilibrium thermodynamic parameters for binding; for adipocyte and heart FABP, the enthalpy of binding becomes more favorable with increasing FA unsaturation and, correspondingly, the entropy becomes less favorable, while for intestinal FABP the enthalpy is roughly constant for all FA, but the entropy term becomes less favorable with increasing unsaturation (14).

Although structural and binding studies provide insight into the interactions of FA and FABP at equilibrium, they leave unanswered questions concerning the kinetic features of these reactions, which are key to understanding a number of functional and structural properties of the FABPs. Determination of the rates of binding and dissociation of FA from FABPs is essential for understanding the kinetic constraints that govern intracellular FA trafficking and metabolism and the mechanism by which FA enter and leave the FABP binding cavity. Measurements of the rate constants and their temperature dependence should provide information about the thermodynamic parameters of the activation barrier for entering and leaving the binding site and the comparison of rate constants for site-specific mutants will provide information about how FA gain access to the binding cavity.

With the exception of our initial results discussed in Refs. 12 and 14, no measurement of the kinetics of FA-FABP binding and dissociation have been reported. However, Storch and colleagues (15–17) have carried out extensive measurements of the transfer of the chemically modified anthroyloxy-FA from FABPs to membranes. These measurements revealed considerable heterogeneity among the FABPs both in the rates and in the transfer mechanism itself. These AOFA results together with our results for unmodified FA and FABPs (12, 14), suggest that rate constants for binding and dissociation of unmodified FA are also sensitive functions of FA and FABP type.

In the present study we have determined the rate constants for the binding of a set of unmodified FA to the fluorescently labeled I-FABP, ADIFAB. ADIFAB, which exhibits distinct fluorescence spectra in the FA-bound and FA-unbound states, was then used to monitor the rate of dissociation of FA from adipocyte, heart, and intestinal FABPs. We also report the development of a new higher affinity FFA probe, ADIFAB2, and describe its use in determining rate constants for higher affinity FA-FABP interactions. The measured dissociation rate constants (k_{off}) were used to calculate k_{on} values from k_{on} =

* This work was supported by National Institutes of Health Grant GM46931. The costs of publication of this article were defrayed in part by the payment of page charges. This article must therefore be hereby marked "*advertisement*" in accordance with 18 U.S.C. Section 1734 solely to indicate this fact.

‡ To whom correspondence and reprint requests should be addressed: Medical Biology Institute, 11077 N. Torrey Pines Rd., La Jolla, CA 92037.

[1] The abbreviations used are: FABP, fatty acid binding protein; AA, arachidonate (20:4); ADIFAB, acrylodated I-FABP; ADIFAB2, acrylodated L72A-I-FABP; FA, fatty acid; FFA, free fatty acids; A-FABP, adipose FABP; MA, myristate (14:0); LA, linoleate (18:2); LNA, linolenate (18:3); OA, oleate (18:1); PA, palmitate (16:0); H-FABP, heart FABP; I-FABP, intestinal FABP; BSA, bovine serum albumin.

k_{off}/K_d, where the equilibrium dissociation constants K_d, were determined previously (12–14). Thermodynamic characteristics of the energy barriers corresponding to binding and dissociation were determined from the temperature dependence of the measured rate constants using Eyring transition-state theory.

EXPERIMENTAL PROCEDURES

Materials—All measurements were done using the sodium salts of the FA purchased from Nu Chek Prep, Elysian, MN, as described previously (12–14). The buffer used to measure FA binding to FABPs consisted of 20 mM HEPES, 150 mM NaCl, 5 mM KCl, and 1 mM $NaHPO_4$, at pH 7.4. All FABPs (rat intestine, human and mouse adipocyte, and rat heart) were recombinant proteins that were expressed in the BL21 (DE3)/pET11 host/vector expression system and proteins were purified from cell lysates by a modification of the method of Lowe *et al.* (18) as described previously (12–14). ADIFAB was prepared from acrylodan-derivatized recombinant rat intestinal fatty acid binding protein as described (13) and is available from Molecular Probes.

ADIFAB2 Construction and Fluorescence Properties—The $Leu^{72} \rightarrow$ Ala variant of I-FABP was obtained as follows. First a restriction fragment, carrying the Ala^{72} mutation and appropriate complementary ends, was substituted for the wild-type restriction fragment spanning the *Sal*I site at position 211 in the I-FABP cDNA sequence (19) and a *Pme*I site at position 291, which we had introduced by site-specific mutagenesis (20). The mutated restriction fragment was constructed by annealing partially complementary synthetic oligonucleotides carrying the desired sequence, "filling in" single stranded regions with the DNA polymerase Klenow fragment, and digesting with *Sal*I and *Pme*I to give the appropriate termini. The Ala^{72} substituted I-FABP cDNA was inserted into the pET11 vector and was expressed in the BL21(DE3) strain. The mutant I-FABP was purified, as described above, and yielded about 100 mg of purified protein per liter of *Escherichia coli* culture. Acrylodan derivatization was done as described previously for ADIFAB (13). Following Lipidex-5000 chromatography to remove free acrylodan, ADIFAB2 was found have an acrylodan:FABP ratio of 1:1.

The fluorescence properties of the acrylodan-derivatized $Leu^{72} \rightarrow$ Ala I-FABP (ADIFAB2) are significantly different than ADIFAB's (data not shown). The positions of the emission maxima occur at longer wavelengths, 440 nm for apo-ADIFAB2 and 550 nm for holo-ADIFAB2, compared to 432 and 505 nm for ADIFAB, and the optimal excitation wavelength is at 375 nm for ADIFAB2 as compared to 386 nm for ADIFAB. These two different sets of excitation and emission wavelengths were used in the present study for measurements using ADIFAB2 and ADIFAB, respectively. Furthermore, the parameters that define the equilibrium binding properties, R_o, R_{max}, and Q of Equation 1 of Ref. 13, are also significantly different for ADIFAB2 and, in contrast to ADIFAB, the values of these parameters are FA and temperature dependent. Thus for oleate, R_{max} and Q range between 1.6 and 2.5, and between 7.5 and 12, respectively, for temperatures between 10 and 37 °C, and these values are all approximately 10% higher for palmitate.

Stopped-flow Fluorescence—Rapid mixing fluorescence was done using an SLM Milliflow stopped-flow device coupled to an SLM 8100 fluorometer (SLM Instruments, Rochester, NY) in which equal volumes (0.1 ml) of reactants were mixed with a dead time of about 5 ms. Fluorometric detection was done using two cooled photomultipliers placed on opposite sides of the viewing chamber (T format) and intensities were monitored through 20-nm band width filters centered at 432 and 505 nm (Omega optical, Brattleboro, VT). A minimum of 3 scans were acquired for each temperature, FA, and FABP, and approximately 1000 data points were collected per scan.

Three separate types of kinetic measurements were done: 1) dissociation of FA from ADIFAB, 2) binding of FA to ADIFAB, and 3) dissociation of FA from FABP. Dissociation of FA from ADIFAB was measured by mixing a solution of FA and ADIFAB in one syringe of the stopped-flow device with excess fatty acid-free BSA in the second syringe. The binding of FA to ADIFAB was measured by mixing solutions of FA in one syringe with ADIFAB in the second syringe. The dissociation of FA from FABP was measured by mixing a solution of FA and FABP in one syringe with ADIFAB in the second syringe.

Kinetic Analysis—The rate constants for each of the three reactions were determined by analyzing the measured time courses with a kinetic model in which transfer of FA from one protein to another proceeds through the aqueous phase, without protein collision. This model is described by the following three equations:

$$\frac{d[\text{ADIFAB}]_b}{dt} = -k_{off}^{AF} \cdot [\text{ADIFAB}]_b + k_{on}^{AF} \cdot [\text{ADIFAB}]_f \cdot [\text{FFA}] \quad \text{(Eq. 1)}$$

$$\frac{d[\text{FFA}]}{dt} = +k_{off}^{AF} \cdot [\text{ADIFAB}]_b + k_{off}^{Prot} \cdot [\text{Protein}]_b - (k_{on}^{AF} \cdot [\text{ADIFAB}]_f + k_{on}^{Prot} \cdot [\text{Protein}]_f) \cdot [FFA] \quad \text{(Eq. 2)}$$

$$\frac{d[\text{Protein}]_b}{dt} = -k_{off}^{Prot} \cdot [\text{Protein}]_b + k_{on}^{Prot} \cdot [\text{Protein}]_f \cdot [\text{FFA}] \quad \text{(Eq. 3)}$$

where FA binding and dissociation are k_{on} and k_{off}, respectively. The off- and on-rate constants for ADIFAB and the FABP or BSA proteins are designated with superscript AF and Prot, respectively. The subscripts b and f designate the FA bound and free concentrations, respectively.

With appropriate boundary conditions, Equations 1–3 describe models used to analyze all three types of kinetic measurements. The initial conditions ($t = 0$) that apply to each of these types of measurements are: 1) for measurements of the off-rate from ADIFAB, [Protein(0)] = 0, and $[\text{ADIFAB}(0)]_b$ and [FFA(0)] are both determined from the equilibrium condition that exists before mixing, using the previously measured equilibrium constants (14); 2) for ADIFAB on-rate measurements, $[\text{ADIFAB}(0)]_b = 0$ and $[\text{FFA}(0)] = [\text{FFA}_{total}]$; and 3) for the FABP off-rate measurements, $[\text{ADIFAB}(0)]_b = 0$, and $[\text{FABP}(0)]_b$ and [FFA(0)] were determined from equilibrium conditions. The solutions to Equations 1–3 yield the concentrations of FA bound ADIFAB, FA bound Protein, and FFA as a function of time.

The quantity that is actually measured in these studies is the time dependent change in the ratio of the fluorescence intensity of ADIFAB at 505 and 432 nm ($R(t)$). To obtain rate constants from these measurements, $R(t)$ must be expressed in terms of the solutions to Equations 1–3, $[\text{ADIFAB}(t)]_b$ and $[\text{FFA}(t)]$. This can be done by expressing the intensities at each wavelength in terms of the contributions of the bound and free forms of ADIFAB as described previously (13, 21, 22). Thus the fluorescence intensity at the emission wavelength λ is given by,

$$I(\lambda) = [\text{ADIFAB}]_b \, I_b(\lambda) + [\text{ADIFAB}]_f \, I_f(\lambda) \quad \text{(Eq. 4)}$$

in which $[\text{ADIFAB}]_b$ and $[\text{ADIFAB}]_f$ are the bound and free concentrations of ADIFAB and $I_b(\lambda)$ and $I_f(\lambda)$ are the specific fluorescence intensities of these components. The ratio of intensities at 505 and 432 nm is therefore the following,

$$R = \frac{[\text{ADIFAB}]_b \cdot I_b(505) + [\text{ADIFAB}]_f \cdot I_f(505)}{[\text{ADIFAB}]_b \cdot I_b(432) + [\text{ADIFAB}]_f \cdot I_f(432)} \quad \text{(Eq. 5)}$$

Dividing the numerator and denominator of the right-hand side of Equation 5 by $[\text{ADIFAB}]_f \cdot I_f(432)$ we obtain,

$$R(t) = \frac{R_o + 0.59 \cdot X(t)}{1 + 0.05 \cdot X(t)} \quad \text{(Eq. 6)}$$

where R_o is the value of R in the absence of FA and the numerical constants were obtained from the spectral properties of ADIFAB as described previously (13), and

$$X(t) = \frac{[\text{ADIFAB}(t)]_b}{[\text{ADIFAB}]_{total} - [\text{ADIFAB}(t)]_b} \quad \text{(Eq. 7)}$$

where $[\text{ADIFAB}]_b$ is a solution of Equations 1–3.

To obtain the rate constants it is necessary to fit the measured $R(t)$ values with the values predicted by Equation 6. The measurements to determine k_{off} from ADIFAB were done in the presence of excess BSA, effectively eliminating the reverse reaction, and therefore for this type of measurement $[\text{ADIFAB}(t)]_b$ is simply,

$$[\text{ADIFAB}]_b(t) = [\text{ADIFAB}]_b(0) e^{-k_{off}^{AF} t} \quad \text{(Eq. 8)}$$

Upon substitution of Equation 8 into Equation 6 an expression for $R(t)$ is obtained that readily can be fitted to measured $R(t)$ values to obtain k_{off}^{AF}. For measurements of type 2 and type 3, Equations 1–3 were solved numerically. Thus for type 2 and 3 measurements, values of the rate constants, initial values, and any other boundary conditions are selected, Equations 1–3 are solved for these values, $R(t)$ is obtained using the numerical values of $[\text{ADIFAB}(t)]_b$, and these calculated $R(t)$ values are then compared with the measured ones. This process was facilitated with the program MLAB (Civilized Software, Bethesda, MD) which

determines the model parameters by using a Marquardt-Levenberg minimization to fit numerical solutions of Equations 1–3 and measured $R(t)$ values. Values obtained by this procedure were verified in selected cases by solving Equations 1–3 using the Runge-Kutta facility of the program Macsyma (Macsyma, Cambridge, MA).

Reliable fitting of the measured scans requires constraints in addition to the initial conditions. Measurements of types 2 and 3 involve bimolecular interactions and therefore the reaction kinetics depend upon the concentration of the reactants. Although the nominal concentrations of FA in the reservoir syringes is known, the actual concentration reaching the mixing chamber exhibits variations from scan to scan because of surface absorption of the FA. To help reduce the uncertainties in the rate constants resulting from these variations, the observed values of the initial and equilibrium values of $R(t)$, R_o, and $R(\infty)$, in each scan were used to define the actual total FA in the mixing chamber using,

$$[\mathrm{FA}]_{\mathrm{total}}(\infty) = [\mathrm{FFA}](\infty) + [\mathrm{ADIFAB}]_b(\infty) + [\mathrm{FABP}]_b(\infty) \quad \text{(Eq. 9)}$$

All three terms on the right-hand side are evaluated using the values of R_o and $R(\infty)$ obtained from the fit, together with the previously measured binding constants (12). Thus from Refs. 12, 13, and 23,

$$[\mathrm{FFA}](\infty) = K_d\ 19.5\ (R(\infty) - R_o)/(11.5 - R(\infty)) \quad \text{(Eq. 10)}$$

$$[\mathrm{ADIFAB}]_b(\infty) = [\mathrm{ADIFAB}]_{\mathrm{total}}\ 19.5\ (R(\infty) - R_o)/(11.5 - R(\infty) + 19.5\ (R(\infty) - R_o)) \quad \text{(Eq. 11)}$$

$$[\mathrm{FABP}]_b(\infty) = \frac{[\mathrm{FABP}]_{\mathrm{total}}}{1 + \dfrac{K_d}{[\mathrm{FFA}](\infty)}} \quad \text{(Eq. 12)}$$

With these constraints, fitting of data for the type 2 measurements was done by allowing k_{on}, R_o, and $R(\infty)$ to vary. For the type 3 measurements the variable parameters were, k_{off} and k_{on}, with the constraint $k_{\mathrm{off}}/k_{\mathrm{on}} = K_d$, R_o, and $R(\infty)$. These procedures resulted in well behaved fitting characteristics in which the fit values of R_o and $R(\infty)$ returned values in agreement with the measured values. The quality of fit was assessed by the sum of squares of the theory experiment differences (SOSQ), fit residuals, and direct observation, and generally gave excellent agreement between theory and experiment, with typical SOSQ values $<1 \times 10^{-2}$.

Limits of Resolution for Determination of Rate Constants for FA Transfer from FABP to ADIFAB—Determination of rate constants relies on the accuracy of the ADIFAB rate constants as well as the characteristics of the kinetic model used to analyze the time course of transfer. To determine how the characteristics of the kinetic model affect the accuracy with which rate constants can be determined, time courses for transfer of FA from FABP to ADIFAB were simulated by solving Equations 1–3 with arbitrary rate constants for FABP and with the measured rate constants for ADIFAB. These simulated transfers reveal, as seen for the example of oleate dissociation from I-FABP in Fig. 1, how the concentration of the three reactants, [ADIFAB$_b$], [FFA], and [FABP$_b$] are expected to vary with time after mixing. These results show that for small k_{off} values FA dissociation from FABP is tightly correlated with an increase in FA bound to ADIFAB and with a monotonic decrease in the concentration of the free FA. For larger FABP off-rate constants, the rate at which FA dissociates from FABP can exceed the rate at which FA can bind to ADIFAB, thereby uncoupling the two processes. This uncoupling is most evident in the time course for [FFA] where, for large k_{off} values, the concentration at early times actually increases before decaying toward equilibrium. This increase occurs because the FA-FABP solution is perturbed from equilibrium by mixing. Immediately after mixing the FA-FABP solution is diluted 2-fold with the ADIFAB solution, and in this diluted solution [FFA] is initially less than the equilibrium value for the FA/FABP mixture but greater than the equilibrium value of the FA/FABP/ADIFAB mixture. This transient increase is not observed at small k_{off} values because the rate of FA binding to ADIFAB is equal to or greater than the rate of dissociation from FABP. At larger k_{off} values, in contrast, appreciable dissociation from FABP occurs, as the FA-FABP system adjusts to its diluted environment, and this occurs more rapidly than the rate of binding to ADIFAB.

These limits on resolution of FABP off-rates are also apparent in the time course of $R(t)$, the quantity actually measured. As Fig. 1*B* indicates, the time course approaches a limiting function as k_{off} increases. The ability of ADIFAB to resolve dissociation rate constants depends upon the experimental uncertainty in $R(t)$ and is a function of both the off-rate from FABP and the FABP's equilibrium constant. In the example of Fig. 1, ADIFAB would resolve k_{off} values $<30\ \mathrm{s}^{-1}$ for I-FABP (K_d = 36 nM). Resolution of off-rate constants from the less tightly binding A-FABP (K_d = 60 nM), however, would be $<50\ \mathrm{s}^{-1}$ (data not shown). This resolving power of ADIFAB is a direct reflection of the rate of response of ADIFAB to FA binding and therefore is proportional to the on-rate constant as well as ADIFAB's binding affinity relative to the donor FABP. Thus ADIFAB2, for which values and binding affinities are larger than for ADIFAB (see below), has been used in the present study to help resolve dissociation in those cases where large k_{off} values and/or small K_d values limit the response rate of ADIFAB.

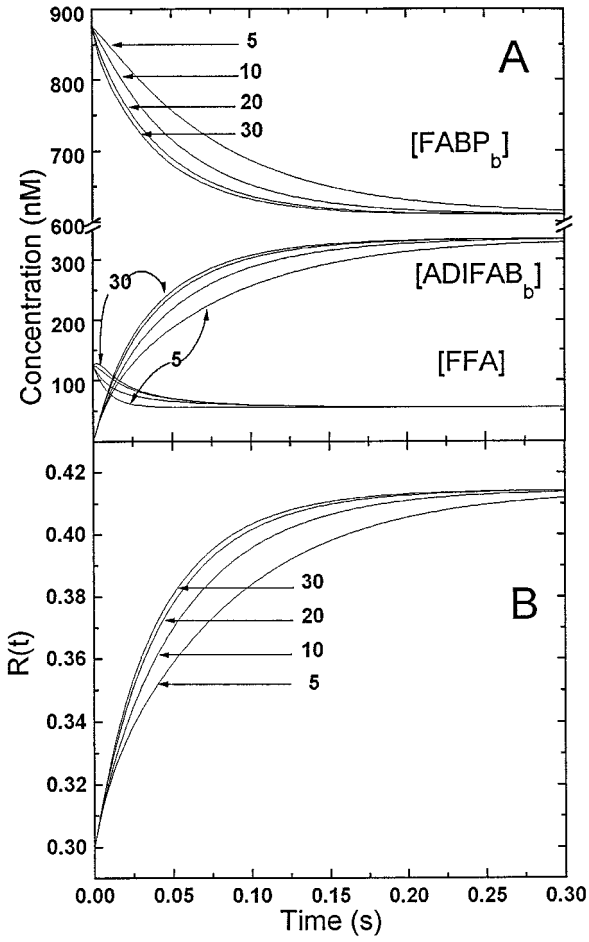

FIG. 1. **Simulations of the dissociation of oleate from I-FABP monitored by ADIFAB fluorescence.** Time courses of oleate dissociation from I-FABP at 37 °C were calculated using the kinetic model described by Equations 1–3. For these simulations the total concentrations of ADIFAB, FABP, and oleate were, respectively, 2, 1, and 1 μM. Rate constants used for ADIFAB (Fig. 3) were $k_{\mathrm{off}} = 10.7\ \mathrm{s}^{-1}$, $k_{\mathrm{on}} = 3.8 \times 10^7\ \mathrm{M}^{-1}\mathrm{s}^{-1}$ and for I-FABP k_{on} was set equal to k_{off}/K_d, where K_d = 30 nM (12) and k_{off} values were varied between 5 and 30 s^{-1} as indicated in the figure. *A*, concentrations of each the reactants ([ADIFAB$_b(t)$], [FFA(t)], [FABP$_b(t)$]) were obtained by solving Equations 1–3 using the Runge Kutta method. *B*, values of the ADIFAB fluorescence intensity ratio were calculated using Equation 6.

Eyring Transition State Theory—Activation thermodynamic parameters were calculated using Eyring rate theory (24) in which rate constants are related to the transition state activation energy as shown below,

$$k = \frac{T\,\kappa \cdot k_B}{h} e^{-\frac{\Delta G^{\ddagger}}{RT}} \quad \text{(Eq. 13)}$$

where T is temperature in degrees of Kelvin, κ is the transmission coefficient and is set to unity in these calculations, k_B is Boltzman's, and h is Planck's constant, and $\Delta G^{\ddagger}$ and is the free energy of activation. The activation enthalpy was determined from the slope of Arrhenius plots of the rate constants as the following,

$$\Delta H\ddagger = -R\left(\frac{d\ln k}{d\left(\frac{1}{T}\right)} + T\right) \quad \text{(Eq. 14)}$$

and the activation entropy was determined as,

$$T\Delta S\ddagger = \Delta H\ddagger - \Delta G\ddagger \quad \text{(Eq. 15)}$$

In using this analysis it is assumed that the thermodynamic model provides a reliable representation of the formation of the transition state and that the activation enthalpies and entropies are temperature independent. Recently, studies of equilibrium reactions have called into question the use of the van't Hoff analysis, and therefore the temperature independence of equilibrium enthalpies and entropies, to determine thermodynamic parameters from binding measurements (25, 26). Whether such reservations apply to the activation parameters is unclear. However, two observations suggest that at least for FA-FABP interactions thermodynamic parameters calculated assuming temperature independence may be accurate. First, as discussed by Weber (25), the errors made in assuming temperature independence may be small when, as is the case in the present study (Table IV), the activation free energies are predominantly enthalpic. Second, the predominance of enthalpy also applies to the equilibrium thermodynamic parameters for FA binding to FABP as determined by both van't Hoff (14) and calorimetry measurements (27, 28), although the van't Hoff determined ΔH are larger (more favorable) by about 3 kcal/mol.

RESULTS

ADIFAB Kinetics—Rate constants for the dissociation of FA from ADIFAB (k_{off}) were determined by measuring the dissociation of FA from ADIFAB using fatty acid-free BSA as a sink. In all cases virtually identical rate constants were obtained using BSA concentrations between 6 and 20 μM, indicating saturating levels of BSA (data not shown). Thus Equation 8 can be used to analyze the dissociation time course and as seen in the example shown in Fig. 2, provides an excellent description of this process. Results of this analysis yield k_{off} values that range from about 0.8 to 50 s^{-1} depending upon temperature and FA type (Table I and Fig. 3*A*). These results show moreover that k_{off} for ADIFAB increases with FA type as OA $\approx$ PA $>$ LA $>$ AA $>$ LNA and for each FA, k_{off} decreases exponentially with decreasing temperature (Fig. 3*A*). This variation of k_{off} with FA type follows, inversely, the variation of FA affinity for ADIFAB described previously (12, 13).

Time courses for binding of FA to ADIFAB were measured by mixing FA and ADIFAB; our results for oleate binding at temperatures between 15 and 37 °C are shown in Fig. 4. Also shown in this figure are the fits to these measured time courses obtained with the kinetic model represented by Equations 1–3. These fits were obtained by allowing both k_{off} and k_{on} to vary with the constraint that $k_{off}/k_{on} = K_d$, where K_d values were those measured previously (12). The results of this analysis as seen in Fig. 3 and Table I, yields k_{on} values that range between 1×10^5 and 5×10^6 $M^{-1}s^{-1}$ and k_{off} values that are virtually identical with those obtained directly from measurements of FA transfer from ADIFAB to BSA described above. As was seen for the time course of dissociation, the rate of binding increases with increasing temperature. However, in contrast to the significant variation of k_{off} with FA type, virtually identical k_{on} values were obtained for all FA (Table I).

Arrhenius plots of the on- and off-rate constants (Fig. 3) were analyzed in terms of Eyring transition state theory which yielded the thermodynamic parameters of activation shown in Table II. As these results indicate, the free energies of activation for dissociation range between about 16 and 17 kcal/mol and show a decrease with increasing double bond number for the 18 carbon length FA. Table II also shows that for all FA the enthalpic portion of the activation energy is significantly larger, between about 12 and 13 kcal/mol, than the entropic component (3–4 kcal/mol). For the binding step the thermodynamic parameters are quite similar for all FA and in particular indicate that the activation barrier is predominantly enthalpic with average $\Delta H^{\ddagger}$ values of about 9.5 kcal/mol (Table II).

Equilibrium and Kinetics of FA Interactions with ADIFAB2—In studies in progress we have been examining how Ala substitutions for amino acid residues that are located within the I-FABP binding cavity affect FA-FABP interactions. In the course of these studies we found that the $Leu^{72} \rightarrow Ala$ (L72A) mutant possessed FA binding affinities that were 10–20-fold greater than the native I-FABP (data not shown). In order to obtain a new higher affinity FFA probe, ADIFAB2 was constructed by derivatizing the L72A mutant of I-FABP with acrylodan. Equilibrium binding properties of ADIFAB2 were determined essentially by the same methods as used previously to characterize ADIFAB (Methods 13). FA dissociation constants found for ADIFAB2 (Fig. 5*A*) ranged between 8 and 50 nM, or 10–20-fold greater affinities than for ADIFAB, consistent with the differences found for the underivatized FABPs. Rate constants for FA interacting with ADIFAB2 were determined by the same methods as for ADIFAB. The results shown in Fig. 5,

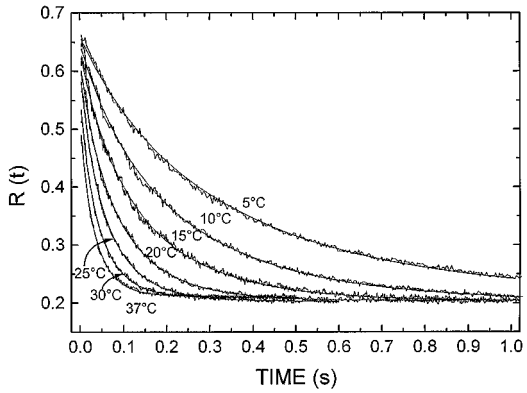

FIG. 2. **Measured time courses for dissociation of linoleate from ADIFAB.** These measurements were done by monitoring the ADIFAB $R(t)$ value after stopped-flow mixing ADIFAB-linoleate complexes with fatty acid-free BSA at temperatures between 5 and 37 °C. Each time course is an average of at least three separate measurements and initial reactant concentrations were: ADIFAB, 1 μM; linoleate, 1 μM; and BSA, 5 μM. *Solid lines* are least squares fits to the data using Equation 8 from which were obtained the k_{off} values plotted in Fig. 3.

TABLE I
On- and off-rate constants at 25 °C

Values for k_{on} are in units of 10^7 $M^{-1}s^{-1}$ and for k_{off} in units of $M^{-1}s^{-1}$. Standard deviations for k_{off} values range from about 15 to 40% for the derivatized and underivatized proteins, respectively. Abbreviations for the FA are: PA, palmitate (16:0); OA, oleate (18:1); LA, linoleate (18:2); LNA, linolenate (18:3); and AA, arachidonate (20:4).

	PA		OA		LA		LNA		AA	
	k_{on}	k_{off}	k_{on}	k_{off}	k_{on}	k_{off}	k_{on}	k_{off}	k_{on}	k_{off}
ADIFAB	1.6	4.6	1.9	4.6	1.5	12	1.0	25	1.7	20
ADIFAB2	5.4	0.8	3.4	1.2						
Adipose-FABP	7.1	5.2	5.8	2.4	4.3	2.8	6.6	7.6	2.8	4.0
Heart-FABP	15	1.1	5.7	0.25	4.2	0.57	2.2	0.82	4.9	1.2
Intestine-FABP	23	1.8	11	1.8	6.9	3.9	11	19	5.7	6.0

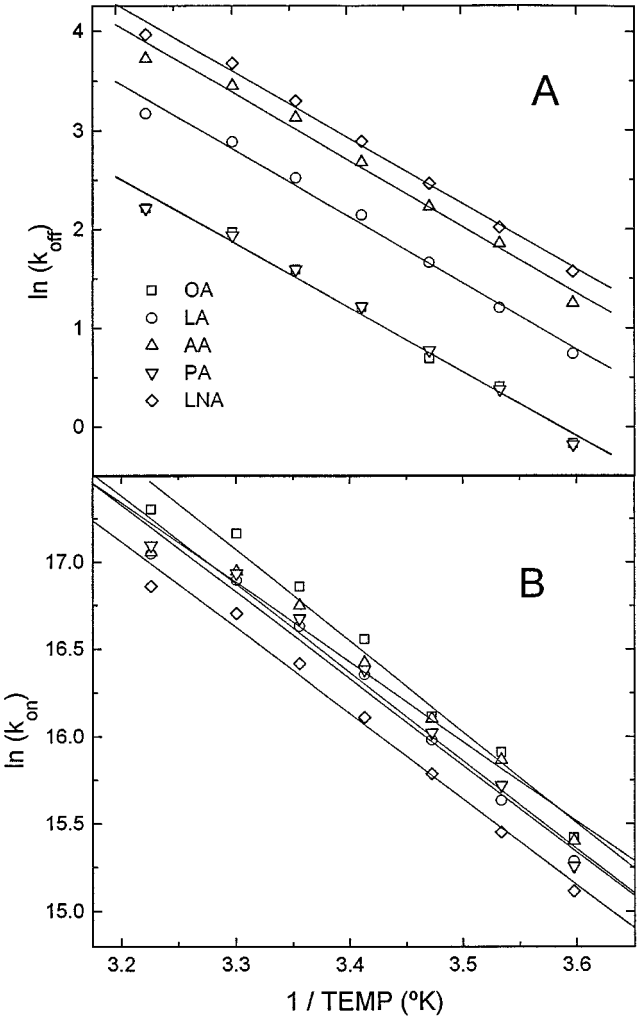

FIG. 3. **Arrhenius plots of ADIFAB off- and on-rate constants.** Measured values are shown as *symbols* and the results of linear regressions are shown as *solid lines* through the data. *A*, $\log_e$ of k_{off}. *B*, $\log_e$ of k_{on}. Abbreviations are as listed in Table I.

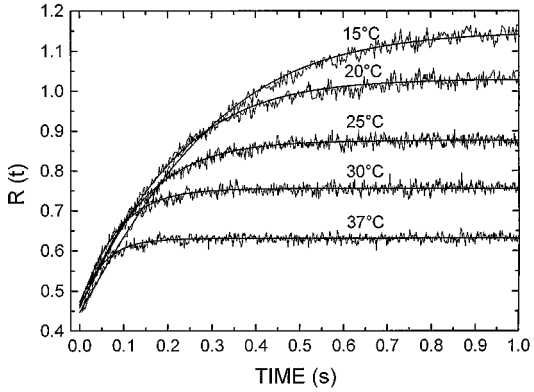

FIG. 4. **Measured time courses for oleate binding to ADIFAB.** The ADIFAB fluorescence ratio ($R(t)$) was monitored following stopped-flow mixing of ADIFAB (1 μM) and oleate (nominal concentration 1 μM) at temperatures between 15 and 37 °C. *Solid lines* are least squares fit to the data using the solutions of Equations 1–3 to obtain the k_{on} values plotted in Fig. 3.

B and *C*, and Table I indicate that k_{off} for ADIFAB2 is about 5-fold smaller than for ADIFAB, while the k_{on} rate constants are generally about 2-fold greater. Because of its faster response time and increased sensitivity for low FFA levels, ADIFAB2 was used to resolve off-rate constants for FA-FABP interactions involving rapid dissociation and/or high affinity such as palmitate and oleate transfer from I-FABP and H-FABP, respectively. Equivalent results were obtained with ADIFAB and ADIFAB2 where, as in the cases of palmitate and oleate transfer from I-FABP both probes could be used to determine transfer rates. Equilibrium and transition state thermodynamic parameters for ADIFAB2 are shown in Table III.

The equilibrium thermodynamic parameters are qualitatively similar to those obtained previously for ADIFAB, showing substantial enthalpic and entropic components; in contrast, for the native I-FABP, enthalpies are about 12 kcal/mol and the entropic components are approximately zero (12). Just as for ADIFAB and the underivatized proteins, the activation free energies for binding to ADIFAB2 (~7 kcal/mol) are dominated by enthalpies which are 8.6 and 10.6 kcal/mol for oleate and palmitate, respectively (Table III). Enthalpies also dominate the dissociation of FA from ADIFAB2, with values that are between ADIFAB (Table II) and I-FABP (Table IV).

Adipocyte-FABP—Time courses for dissociation of palmitate from mouse A-FABP are shown in Fig. 6*A* together with fits to these measurements using the kinetic model represented by Equations 1–3. Time courses for the dissociation of arachidonate from each of the three different native FABPs are shown in Fig. 6*B*. These results are representative of all FA/FABP combinations and illustrate that dissociation from A- and I-FABP is considerably faster than from H-FABP. The results of Fig. 6*A* also show that the rate of dissociation increases with temperature and that between 10 and 37 °C dissociation from A-FABP is complete within about 2 s. A-FABP off-rate constants determined from these as well as from measurements with the other FA are shown as Arrhenius plots in Fig. 7 and are listed in Table I. The k_{off} values for the 18 carbon FA increase with the degree of FA unsaturation and for all FA k_{off} range between about 1 and 20 s^{-1}. Off-rate constants for oleate were also measured using human A-FABP and these values are virtually identical to those found with mouse A-FABP (data not shown). On-rate constants calculated from the k_{off} and previously determined K_d values (12), are shown in Fig. 7*B* and Table I. These results reveal little difference in k_{on} among the different FA. Values for k_{on} increase with temperature and between 10 and 37 °C range from about 1 to 40 $\times$ 10^7 $M^{-1}s^{-1}$, ABOUT 5-FOLD GREATER THAN FOR ADIFAB.

The Arrhenius plots for the A-FABP rate constants were analyzed using the Eyring transition state model (Table IV). The results show that the free energy needed to form the transition state for dissociation (about 17 kcal/mol) is composed of a large enthalpic (13–16 kcal/mol) and a smaller entropic (0–4 kcal/mol) component. Within the uncertainties of these results (1–3 kcal/mol), the thermodynamic parameters are similar for all of the FA. Thermodynamic parameters for the binding step are also similar for all FA and reveal that, with the exception of arachidonate, the activation free energies which are about 8 kcal/mol, are predominantly enthalpic (Table IV).

Heart FABP—Dissociation rates from heart FABP are considerably slower than from adipocyte or intestinal FABP, as exemplified by arachidonate at 25 °C shown in Fig. 6*B*. This result also shows that the change in R value at equilibrium is considerably smaller with H-FABP as compared to A- and I-FABP. This is a direct reflection of the lower equilibrium FFA levels for the higher affinity H-FABP (K_d = 26 nM) than A- and I-FABP (K_d values both about 130 nM). Hence ADIFAB2 was used to measure palmitate and oleate dissociation from H-FABP because of its significantly higher affinity as compared to ADIFAB. The measured off-rate constants for heart FABP range between 0.2 and 3 s^{-1} for the 5 different FA and are shown as Arrhenius plots in Fig. 8*A* and Table I. On-rate

TABLE II
Eyring transition state analysis of ADIFAB off-rate constants

Abbreviations as listed in Table I.

	PA	OA	LA	LNA	AA
ADIFAB on-step parameters					
$\Delta G‡$	7.7 ± 0.1[a]	7.6 ± 0.1	7.7 ± 0.1	8.0 ± 0.1	7.7 ± 0.1
$\Delta H‡$	9.5 ± 0.7	9.8 ± 0.7	9.3 ± 0.6	9.2 ± 0.5	8.5 ± 0.7
$-T\Delta S‡$	−1.8 ± 0.5	−2.3 ± 0.5	−1.6 ± 0.4	−1.2 ± 0.4	−0.9 ± 0.5
ADIFAB off-step parameters					
$\Delta G‡$	16.7 ± 0.1	16.7 ± 0.1	16.1 ± 0.1	15.7 ± 0.1	15.8 ± 0.1
$\Delta H‡$	12.5 ± 0.6	12.5 ± 0.7	12.9 ± 0.6	12.7 ± 0.5	12.9 ± 0.7
$T\Delta S‡$	4.2 ± 0.4	4.2 ± 0.5	3.2 ± 0.4	2.9 ± 0.4	2.9 ± 0.5

[a] All $\Delta G‡$ and $T\Delta S‡$ values were calculated at 25 °C. Energies are in kcal/mol. Standard deviations of 15 and 20% were used for ADIFAB off- and on-rate constants, respectively. Uncertainties (S.D.) for each of the thermodynamic parameters were calculated, by using standard error propagation rules (34), as 0.6 $\delta k/k$, where δk is the standard deviation of the rate constant k, 2 δslope, and 0.6 $\delta k/k$ + δslope for $\Delta G‡$; $\Delta H‡$, and $T\Delta S‡$, respectively.

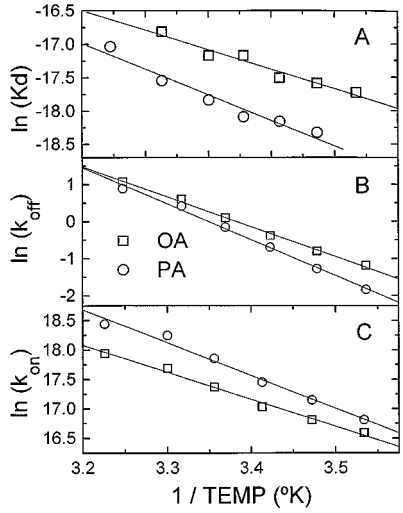

FIG. 5. **van't Hoff plots of the equilibrium and Arrhenius plots of the rate constants for ADIFAB2.** Equilibrium measurements were done as described previously for ADIFAB (13) and rate constants were determined by the same methods as for ADIFAB. *A*, equilibrium dissociation constants for palmitate and oleate. *B* and *C*, off- and on-rate constants for palmitate and oleate. Measured values are shown as *symbols* and the results of linear regressions are shown as *solid lines* through the data.

TABLE III
ADIFAB2 equilibrium and EYRING transition state analysis

Abbreviations, units, and conditions as described in Tables I and II.

	PA	OA
ADIFAB2 equilibrium parameters		
ΔG	10.8 ± 0.1	10.4 ± 0.1
ΔH	6.3 ± 0.6	5.9 ± 0.6
$T\Delta S$	4.5 ± 0.6	4.5 ± 0.6
ADIFAB2 on-step parameters		
$\Delta G‡$	7.0 ± 0.1	7.3 ± 0.1
$\Delta H‡$	10.6 ± 0.7	8.6 ± 0.4
$-T\Delta S‡$	−3.6 ± 0.5	−1.4 ± 0.5
ADIFAB2 off-step parameters		
$\Delta G‡$	17.7 ± 0.1	17.5 ± 0.1
$\Delta H‡$	17.6 ± 0.6	14.5 ± 0.4
$-T\Delta S‡$	0.1 ± 0.7	2.9 ± 0.5

constants calculated from these off-rate constants and the previously measured K_d values range between about 1 and 20 × 10^7 $M^{-1}s^{-1}$. These results are also shown as Arrhenius plots in Fig. 8*B*. The variation of rate constants with FA type generally reflects the behavior expected from the K_d values. For example off-rate constants for the unsaturated FA increase with K_d. Although much of the variation in K_d can be attributed to variations in k_{off}, especially large k_{on} values result in high affinities for palmitate (Fig. 8 and Table I). Eyring transition state analysis of the results of Fig. 8 are shown in Table IV. These results indicate that the activation free energy of FA dissociation is about 18 kcal/mol and is virtually all enthaplic. Although the magnitude of the barriers are considerably smaller ($\Delta G‡$ is about 7 kcal/mol), the on-rate activation pathway is also predominantly enthalpic.

Intestinal-FABP—An example of a typical time course for dissociation of FA from I-FABP is shown in Fig. 6*B* where it is seen that dissociation occurs with similar kinetics as for A-FABP but is considerably faster than for H-FABP. This behavior of I-FABP relative to A- and H-FABPs also applies to the other 4 FA as seen in Table I and Fig. 9*A*, where the k_{off} values determined for I-FABP are displayed as Arrhenius plots. This figure also shows that for palmitate and oleate similar values for k_{off} are obtained using either ADIFAB or ADIFAB2. The corresponding k_{on} values calculated for I-FABP are shown in Fig. 9*B*, where it is seen that these values are about 2- and 10-fold larger than those for H- and A-FABP, respectively. Thermodynamic parameters for the activated state obtained from these measured rate constants are shown in Table IV. Just as for the other proteins, the free energy for the binding and dissociation barriers are dominated by enthalpic contributions. With the exception of the dissociation of palmitate, $\Delta H‡$ values are between 15 and 19 kcal/mol and the corresponding entropic contributions are generally close to zero. Palmitate in contrasts reveals a $\Delta H‡$ value of 24 kcal/mol, the largest value observed in this study and a compensatory (favorable) entropic contribution of 7 kcal/mol. Thermodynamic parameters for the on-step reveal, in contrast to the other FABPs, a significant trend with double bond number; the $\Delta H‡$ values decrease from 10 to 4 kcal/mol, while the $-T\Delta S‡$ values increase monotonically from −4 to 3 kcal/mol.

DISCUSSION

In the present study we have determined on- and off-rate constants as a function of temperature for binding of five of the physiologically most important FA to ADIFAB, ADIFAB2, adipocyte, heart, and intestinal FABPs. In all cases the FA-FABP equilibrium is rapid, occurring within about 2 s and 20 s at 37 and 10 °C, respectively. Off-rate constants varied by about 10-fold among the different FABPs, where k_{off} values were smallest for H-FABP and largest for A-FABP. On-rate constants are 10–100-fold smaller than the values predicted for diffusion limited rates, indicating a significant activation barrier for binding and these values also varied by about 10-fold among the different FABPs. The results demonstrate that the kinetic basis for achieving equilibrium is different in different FABPs; the larger affinity of I- and H-FABPs as compared to

TABLE IV
Activation thermodynamics for native FABPS

Standard deviations of 30 and 40% were used for FABP off- and on-rate constants, respectively. All other conditions, abbreviations, and units as in Tables I and II.

	PA	OA	LA	LNA	AA
Adipose on-step parameters					
$\Delta G‡$	6.8 ± 0.2	6.9 ± 0.2	7.1 ± 0.2	6.9 ± 0.2	7.4 ± 0.2
$\Delta H‡$	9 ± 3	7 ± 2	9 ± 1	9 ± 1	3 ± 1
$T\Delta S‡$	−2 ± 2	−0 ± 1	−2 ± 1	−2 ± 1	4 ± 1
Adipose off-step parameters					
$\Delta G‡$	16.6 ± 0.2	17.1 ± 0.2	17.0 ± 0.2	16.4 ± 0.2	16.8 ± 0.2
$\Delta H‡$	16 ± 2	13 ± 3	15 ± 1	15 ± 1	13 ± 1
$T\Delta S‡$	0 ± 1	4 ± 2	2 ± 1	2 ± 1	4 ± 1
Heart on-step parameters					
$\Delta G‡$	6.4 ± 0.2	6.7 ± 0.2	7.0 ± 0.2	7.5 ± 0.2	7.0 ± 0.2
$\Delta H‡$	13 ± 3	13 ± 2	11 ± 3	7 ± 1	6 ± 2
$T\Delta S‡$	−7 ± 2	−6 ± 1	−4 ± 2	1 ± 1	1 ± 1
Heart off-step parameters					
$\Delta G‡$	17.5 ± 0.2	18.4 ± 0.2	17.9 ± 0.2	17.7 ± 0.2	17.5 ± 0.2
$\Delta H‡$	17 ± 2	18 ± 2	18 ± 2	16 ± 2	16 ± 2
$T\Delta S‡$	0 ± 1	1 ± 1	0 ± 1	2 ± 1	2 ± 1
Intestine on-step parameters					
$\Delta G‡$	6.1 ± 0.2	6.6 ± 0.2	6.8 ± 0.2	6.6 ± 0.2	6.9 ± 0.2
$\Delta H‡$	10 ± 3	9 ± 3	6 ± 1	5 ± 3	4 ± 2
$T\Delta S‡$	−4 ± 2	−2 ± 2	1 ± 1	1 ± 2	3 ± 1
Intestine off-step parameters					
$\Delta G‡$	17.2 ± 0.2	17.2 ± 0.2	16.8 ± 0.2	15.8 ± 0.2	16.5 ± 0.2
$\Delta H‡$	24 ± 2	19 ± 3	18 ± 2	17 ± 2	15 ± 2
$T\Delta S‡$	−7 ± 1	−2 ± 2	−1 ± 1	−1 ± 1	2 ± 1

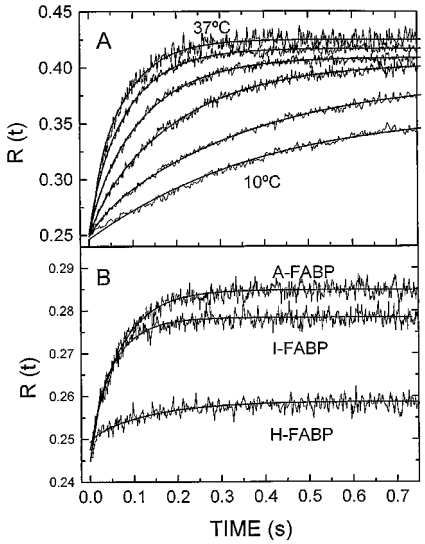

FIG. 6. **Measured time courses for FA dissociation from underivatized FABPs monitored by ADIFAB fluorescence.** Total reactant concentrations in all measurements were: ADIFAB, 2 μM; FABP, 1 μM; and FA, 1 μM. *A*, dissociation of palmitate from human A-FABP monitored with ADIFAB at 5 °C intervals for temperatures between 10 and 30 °C and at 37 °C. *Solid lines* are least squares fits to the data using Equations 1–3 and k_{off} values determined from this analysis are plotted in Fig. 7. *B*, dissociation of arachidonate from A-FABP, H-FABP, and I-FABP at 25 °C. Fits to these data using the kinetic model were used to obtain the k_{off} values shown in Table I.

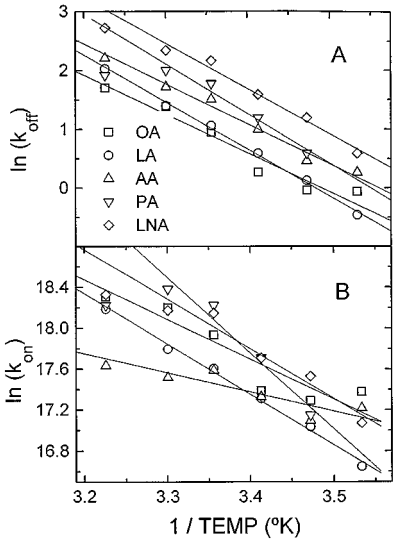

FIG. 7. **Arrhenius plots of A-FABP off- and on-rate constants.** Measured values are shown as *symbols* and the results of linear regressions are shown as *solid lines* through the data. Values for k_{on} were calculated using the measured k_{off} values and K_d values from Ref. 14. *A*, $\log_e$ of k_{off}. *B*, $\log_e$ of k_{on}. Abbreviations are as listed in Table I.

A-FABP are primarily a reflection of larger k_{on} values for I-FABP and smaller k_{off} values for H-FABP. For the native FABPs the activation free energies corresponding to these kinetic processes are primarily enthalpic and are of similar magnitude, suggesting that the activation state for entering or leaving the binding site may involve a common protein structural change. In the following we discuss how the results of the present study can be used to provide insight about the nature of the transition state.

ADIFAB—The Eyring transition state model yields an activation barrier for binding FA to ADIFAB that is composed of an unfavorable enthalpy change, of about 9 kcal/mol, and a favorable 1–2 kcal/mol entropic contribution (Table II). Several observations suggest that the formation of this transition state involves a change in the orientation of the acrylodan moiety and an interaction between FA and ADIFAB. First, acrylodan is probably involved in the transition because derivatization of I-FABP with acrylodan reduces significantly the rate constant for binding FA (Table I). Second, as discussed previously (13) the transition from the apo to holo state of ADIFAB involves a

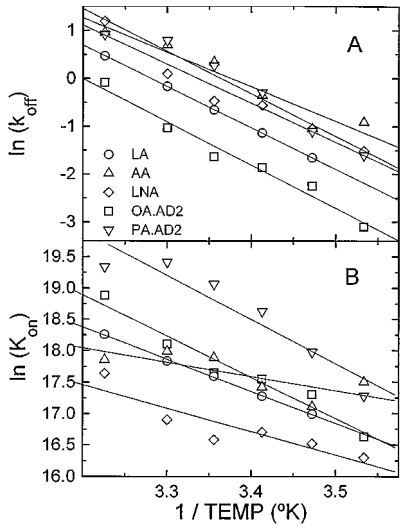

FIG. 8. **Arrhenius plots of H-FABP off- and on-rate constants.** Measured values are shown as *symbols* and the results of linear regressions are shown as *solid lines* through the data. Values for k_{on} were calculated using the measured k_{off} values and K_d values from Ref. 14. *A*, $\log_e$ of k_{off}. *B*, $\log_e$ of k_{on}. *AD2* indicates that these measurements were done using ADIFAB2 and other abbreviations as in Table I.

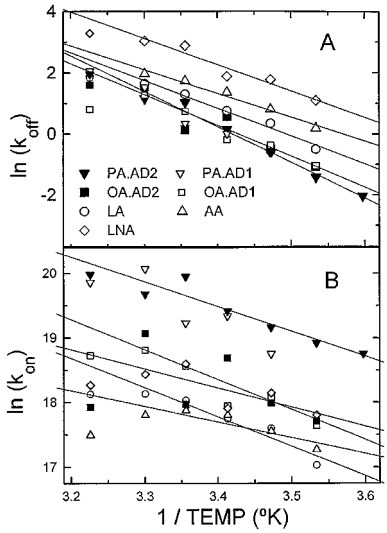

FIG. 9. **Arrhenius plots of I-FABP off- and on-rate constants.** Measured values are shown as *symbols* and the results of linear regressions are shown as *solid lines* through the data. Values for k_{on} were calculated using the measured k_{off} values and K_d values from Ref. 14. *A*, $\log_e$ of k_{off}. *B*, $\log_e$ of k_{on}. *AD1* and *AD2* indicates that these measurements were done using ADIFAB and ADIFAB2, respectively, and other abbreviations as in Table I.

change in acrylodan orientation from one that is tightly bound in an environment of low polarity to one in which the acrylodan moiety is highly mobile and in which the environment is highly polar. This suggests that the transition state may be one in which acrylodan is in an orientation intermediate between its orientation in the apo and holo states. Third, formation of the transition state likely involves the FA because $\Delta H^{\ddagger}$ is FA dependent, decreasing monotonically from 9.8 kcal/mol for oleate to 8.5 kcal/mol for arachidonate (Table II). Fourth, measurements of the acrylodan anisotropy and emission spectra in the apo and holo states of ADIFAB indicate that formation of the holo orientation of acrylodan does not occur with high frequency in the absence of FA. In particular, using the rule for addition of anisotropies (35) together with the previously measured values (13), we estimate that the holo orientation contributes less than 3% of the observed anisotropy in the absence of FA. Thus we speculate that the transition state involves the breaking of bonds between the acrylodan ring structure and amino acid residues that form a low polarity environment and the simultaneous binding of the FA, perhaps to a region between the acrylodan moiety and these amino acid residues. The favorable entropic contribution to the formation of the transition state free energy may involve an increase in mobility for the acrylodan moiety where it is less tightly bound than in the apo state, as well as a contribution from FA and the bulk solvent. Although the free energy of transfer of FA from water to the protein involves an approximately 10 kcal/mol favorable entropic contribution from the bulk solvent (12) this is partially compensated for by decreased internal FA mobility (12) and presumably this loss in FA mobility also occurs when the FA is bound in the transition state. The net activation entropy which decreases in magnitude by about 1 kcal/mol from oleate to arachidonate (Table II) is consistent with the variation in free energy of solubility for these FA (12).

Once in the transition state, the FA·ADIFAB complex can convert to the holo state where FA is bound within the internal cavity of the FABP and the acrylodan moiety is highly mobile and in a polar environment. As Table II indicates, the activation enthalpy for the formation of the transition state from the holo state is constant with FA type and unfavorable by about 12.6 kcal/mol. Because the equilibrium enthalpy is about 3–4 kcal/mol (12) the remaining 9 kcal/mol is used to reform the transition state, consistent with the binding activation parameters. The entropic contribution to activate the transition state upon dissociation is also unfavorable and varies from about 4 for the saturated and mono-unsaturated FA to 3 kcal/mol for the unsaturated FA. At least part of this entropic cost may be due to the reduction in rotational mobility of the acrylodan as it reorients from the highly mobile holo state to the transition state. For example, if the transition were from a rotationally isotropic to immobile state, the entropic loss would be about 2 kcal/mol (36).

The characteristics of ADIFAB2 are consistent with a qualitatively similar transition state as for ADIFAB. ADIFAB2 does, however, exhibit an approximately 0.5 kcal/mol smaller activation free energy for binding as compared to ADIFAB. This smaller energy of activation is consistent with the observed longer emission wavelength maximum in the apo state; 440 nm for ADIFAB2 as compared to 432 nm for ADIFAB (data not shown), assuming that the acrylodan moiety binds less tightly to regions of higher polarity. The substantially larger activation free energy for dissociation from ADIFAB2 (1 kcal/mol greater than for ADIFAB) is consistent with the greater FA affinities for the underivatized L72A-I-FABP as compared to the wild type protein. The smaller entropies for dissociation may also be a reflection of the weaker binding of acrylodan in ADIFAB2, the holo to transition state decrease in entropy being smaller than in the case of the more tighter binding and therefore more constrained ADIFAB.

These results for ADIFAB and ADIFAB2 are consistent with the suggestion that the acrylodan moiety must be displaced in order for FA to gain entry to the ADIFAB binding cavity (13). Based upon an examination of the x-ray crystallographic structure of I-FABP, Sacchettini *et al.* (29) have suggested that a specific region ("portal") at the surface of the protein serves as the entry port for FA access to the binding cavity. The current study provides support for this suggestion because the acrylodan moiety is attached to I-FABP at position 27, which is one of the residues that forms the orifice defining the portal region, and this attachment reduces the k_{on} values by approximately 5–10-fold relative to the underivatized I-FABP (Table I).

Native-FABPs—Activation energies of binding and dissocia-

tion for native adipocyte, heart, and intestinal FABPs are quite similar to one another, suggesting that the transition state for these proteins share common features. For example, the activation free energies for binding, averaged over all 5 FA, are, respectively, 7.0 ± 0.2, 6.9 ± 0.4, and 6.6 ± 0.3 kcal/mol for adipocyte, heart, and intestine, respectively (Table IV). This similarity among the native FABPs is also apparent from the activation thermodynamic parameters of the off-step where it is seen that the free energy change is primarily an enthalpic one of about 16 kcal/mol, the entropic contributions being, on average, about zero. These results do not identify the common structural features that might be involved in the transition state. However, a portal region has been identified at similar locations in all of these proteins (6) and because attachment of acrylodan in this region significantly reduces k_{on} (Table I), we speculate that the transition state might involve the portal region. This speculation is supported by preliminary studies in which site-specific mutations of residues that form the portal region have been found to affect both k_{on} and k_{off} in I-FABP mutants (data not shown). The diameter of the orifice of the portal region that allows access to the binding cavity is about the same as the FA (6, 29). The transition state might therefore involve a fluctuation in the diameter of the orifice which would alternately open and close access to the binding site. Although these putative fluctuations might occur spontaneously, both heart and intestine reveal a significant dependence of the activation enthalpy on FA type, suggesting that at least for these FABPs, the transition state may also involve a FA-FABP interaction.

Although the native FABPs may share a common type of transition state, several aspects of the kinetic and equilibrium results suggest that this state is distinctly different for the acrylodan derivatives of I-FABP and, additionally that acrylodan derivatization perturbs the FA-FABP interactions within the binding cavity. Obviously if acrylodan is involved in the transition state of the derivatized proteins then this state is *per se* different than for the native proteins. Further evidence that these states are different are: 1) the average activation free energy for FA binding to ADIFAB is 1.1 kcal/mol greater than for the native protein, and 2) the binding activation enthalpy (9.5 kcal/mol) for ADIFAB is, with the exception of arachidonate, independent of FA type while $\Delta H^{\ddagger}$ for I-FABP reveals a monotonic decrease from 10 to 4 kcal/mol from palmitate to arachidonate. These results suggest that if the orifice presents a barrier for access to the cavity in the native protein, that derivatization of Lys^{27}, one of the key residues within the portal structure alters the structure of this region so that the orifice does not present a rate-limiting barrier in the derivatized protein. Differences between ADIFAB and I-FABP are particularly evident in the activation enthalpies for dissociation for which ADIFAB reveals a virtually constant value of 12.7 kcal/mol for each of the FA while for I-FABP $\Delta H^{\ddagger}$ decreases monotonically from 24 to 15 kcal/mol from palmitate to arachidonate. These results suggest that derivatization affects interactions within the binding cavity, consistent with the equilibrium results which indicate that the free energy of binding to I-FABP is almost entirely enthalpic while for ADIFAB the equilibrium free energy is composed of appreciable admixtures of entropic and enthalpic components.

Comparison with AOFA Kinetics—Storch and colleagues (17) have studied the transfer of the AOFA from adipocyte, heart, and liver FABPs to lipid membranes. These studies reveal that while transfer of the AOFA from liver FABP to membranes likely occurs through the intervening aqueous phase, transfer from the adipocyte and heart FABPs appears to be mediated by processes than involve direct FABP-membrane interactions. The rate constants determined in these studies might not be comparable directly to those determined in the present study because the AOFA-FABP interactions differ significantly from the unlabeled FA-FABP interactions; equilibrium dissociation constants for example, are about 1–2 orders of magnitude greater for the AOFA (30, 31) than for the unlabeled FA (12). Moreover, the rates for transfer of AOFA from FABP to acceptor membranes might be different than those for the dissociation of the unlabeled FA into the aqueous phase. Nevertheless, rate constants and activation thermodynamic parameters for dissociation of the unlabeled FA are in good agreement with those found for the AOFA by Storch and colleagues (32, 33). The rate constant from these studies for 2-AO-palmitate or stearate transfer from heart FABP, extrapolated to zero acceptor membrane concentration, is about 0.5 s^{-1} at 25 °C, similar to the values found for the dissociation of unlabeled FA from H-FABP in the present study (Table I). For similar transfer conditions and AOFAs, transfer rates from adipocyte FABP were found to be about 10-fold greater than from heart FABP (17), similar to the k_{off} results shown in Figs. 7 and 8 for the unlabeled FA. Finally, thermodynamic parameters found for the transfer of 2-AO-palmitate from adipocyte and heart FABP to lipid vesicles (32, 33) were similar to those found in the present study both in their predominantly enthalpic character and in their magnitude. That such different molecules reveal similar dissociation characteristics is surprising, a detailed understanding of this issue will require more information than is currently available about the structure of AOFA bound to FABP (37). Because of their significantly smaller affinities we estimate k_{on} values for the AOFA are about 10–100-fold lower than for the unlabeled FA, possibly reflecting the greater difficulty for passage of the AOFA through the relatively small orifice defined by the portal region. How interactions with acceptor membranes might affect dissociation of unlabeled FA is unclear, although results comparing rate constants determined for H-FABP with varying ADIFAB and H-FABP concentrations in the present study indicate that collisions between the ADIFAB acceptor and FABPs do not affect dissociation rates (data not shown).

Summary—This study shows that while FABPs reveal considerable variation in binding affinities and rates of response most of this variability results from changes in the rates of dissociation, suggesting that the (transition) mechanism by which FA gain entry to the binding cavity is similar in each of these three FABPs. More detailed understanding of the nature of this mechanism awaits the results of site-specific mutational studies now in progress. We speculate that the rate constants determined in this study have physiologic significance for FA metabolism because the rate at which adipocyte and intestinal FABPs respond to changes in FFA levels is considerably greater than that for the heart FABP. What makes this result potentially relevant for physiology is that both adipose and intestine are concerned with bi-directional intra- to extracellular transport of FA and might be expected to respond rapidly to alterations of FFA levels, whereas in the heart where FA are the major energy substrate, FA transport is presumably unidirectional.

REFERENCES

1. Ockner, R. K., Manning, J. A., Poppenhausen, R. B., and Ho, W. K. L. (1972) *Science* **177,** 56–58
2. Mishkin, S., Stein, L., Fleischner, G., Gatmaitan, Z., and Arias, I. M. (1975) *Am. J. Physiology* **228,** 1634–1640
3. Bass, N. M. (1988) *Intern. Rev. Cytol.* **111,** 143–184
4. Veerkamp, J. H., Peeters, R. A., and Maatman, R. G. H. J. (1991) *Biochim. Biophys. Acta* **1081,** 1–24
5. Veerkamp, J., Maatman, R., and Prinsen, C. (1992) *Biochem. Soc. Trans.* **20,** 801–805
6. Banaszak, L., Winter, N., Xu, Z., Bernlohr, D. A., Cowan, S., and Jones, T. A. (1994) *Adv. Protein Chem.* **45,** 89–151

7. Sacchettini, J. C., and Gordon, J. I. (1993) *J. Biol. Chem.* **268,** 18399–18402
8. Haunerland, N. H., Jacobson, B. L., Wesenberg, G., Rayment, I., and Holden, H. M. (1994) *Biochemistry* **33,** 12378–12385
9. Sacchettini, J. C., Scapin, G., Gopaul, D., and Gordon, J. I. (1992) *J. Biol. Chem.* **267,** 23534–23545
10. Zanotti, G., Scapin, G., Spadon, P., Veerkamp, J. H., and Sacchettini, J. C. (1992) *J. Biol. Chem.* **267,** 18541–18550
11. Xu, Z., Bernlohr, D. A., and Banaszak, L. J. (1993) *J. Biol. Chem.* **268,** 7874–7884
12. Richieri, G. V., Ogata, R. T., and Kleinfeld, A. M. (1994) *J. Biol. Chem.* **269,** 23918–23930
13. Richieri, G. V., Ogata, R. T., and Kleinfeld, A. M. (1992) *J. Biol. Chem.* **267,** 23495–23501
14. Richieri, G. V., Ogata, R. T., and Kleinfeld, A. M. (1995) *J. Biol. Chem.* **270,** 15076–15084
15. Storch, J., and Bass, N. M. (1990) *J. Biol. Chem.* **265,** 7827–7831
16. Wootan, M. G., and Storch, J. (1994) *J. Biol. Chem.* **269,** 10517–10523
17. Storch, J. (1993) *Mol. Cell. Biochem.* **123,** 45–53
18. Lowe, J. B., Sacchettini, J. C., Laposata, M., McQuillan, J. J., and Gordon, J. I. (1987) *J. Biol. Chem.* **262,** 5931–5937
19. Alpers, D. H., Strauss, A. W., Ockner, R. K., Bass, N. M., and Gordon, J. I. (1984) *Proc. Natl. Acad. Sci U. S. A.* **81,** 313–317
20. Inouye, S., and Inouye, M. (1987) in *Synthesis and Applications of DNA and RNA* (Narang, S., ed) pp. 181–204, Academic Press, New York
21. Grynkiewicz, G., Poenie, M., and Tsien, R. Y. (1985) *J. Biol. Chem.* **260,** 3440–3450
22. Richieri, G. V., and Kleinfeld, A. M. (1995) *J. Lipid Res.* **36,** 229–240
23. Anel, A., Richieri, G. V., and Kleinfeld, A. M. (1993) *Biochemistry* **32,** 530–536
24. Eisenberg, D., and Crothers, D. (1979) *Physical Chemistry with Applications to the Life Sciences,* 1st Ed., The Benjamin/Cummings Publishing Company, Inc., Menlo Park, CA
25. Weber, G. (1995) *J. Phys. Chem.* **99,** 1052–1059
26. Naghibi, H., Tamura, A., and Sturtevant, J. M. (1995) *Proc. Natl. Acad. Sci. U. S. A.* **92,** 5597–5599
27. Jakoby, M. G., Miller, K. R., Toner, J. J., Bauman, A., Cheng, L., Li, E., and Cistola, D. P. (1993) *Biochemistry* **32,** 872–878
28. LaLonde, J. M., Levenson, M. A., Roe, J. J., Bernlohr, D. A., and Banaszak, L. J. (1994) *J. Biol. Chem.* **269,** 25339–25347
29. Sacchettini, J. C., Gordon, J. I., and Banaszak, L. J. (1989) *J. Mol. Biol.* **208,** 327–339
30. Storch, J., Bass, N. M., and Kleinfeld, A. M. (1989) *J. Biol. Chem.* **264,** 8706–8712
31. Wootan, M. G., Bass, N. M., Bernlohr, D. A., and Storch, J. (1990) *Biochemistry* **29,** 9305–9311
32. Kim, H.-K., and Storch, J. (1992) *J. Biol. Chem.* **267,** 20051–20056
33. Wootan, M. G., Bernlohr, D. A., and Storch, J. (1993) *Biochemistry* **32,** 8622–8627
34. Bevington, P. R., and Robinson, D. K. (1992) *Data Reduction and Error Analysis for the Physical Sciences,* Second Ed., McGraw-Hill, Inc., New York
35. Weber, G. (1952) *Biochemistry* **51,** 145–167
36. Finkelstein, A. V., and Janin, J. (1989) *Protein Eng.* **3,** 1–3
37. Sha, R. S., Kane, C. D., Xu, Z., Banaszak, L. J., and Bernlohr, D. A. (1993) *J. Biol. Chem.* **268,** 7885–7892